THE JOURNAL OF BIOLOGICAL CHEMISTRY VOL. 287, NO. 18, pp. 14734–14748, April 27, 2012

Imaging P2X4 Receptor Lateral Mobility in Microglia

*REGULATION BY CALCIUM AND p38 MAPK**

Received for publication, December 1, 2011, and in revised form, February 14, 2012 Published, JBC Papers in Press, March 5, 2012, DOI 10.1074/jbc.M111.329334

Estelle Toulme[‡1] **and Baljit S. Khakh**[‡§2]

From the Departments of [‡]*Physiology and* [§]*Neurobiology, David Geffen School of Medicine, UCLA, Los Angeles, California 90095*

Background: P2X4 receptors are ATP-gated ion channels that are expressed in microglia.
Results: P2X4 receptors in microglial processes display distinct types of lateral mobility that is regulated by ATP and by the activated state of microglia.
Conclusion: P2X4 receptor lateral mobility is a regulated process.
Significance: Regulation of P2X4 lateral mobility may be important in neuropathic pain, when microglia become activated.

ATP-gated ionotropic P2X4 receptors are up-regulated in activated microglia and are critical for the development of neuropathic pain, a microglia-associated disorder. However, the nature of how plasma membrane P2X4 receptors are regulated in microglia is not fully understood. We used single-molecule imaging to track quantum dot-labeled P2X4 receptors to explore P2X4 receptor mobility in the processes of resting and activated microglia. We find that plasma membrane P2X4 receptor lateral mobility in resting microglial processes is largely random, consisting of mobile and slowly mobile receptors. Moreover, lateral mobility is P2X subunit- and cell-specific, increased in an ATP activation and calcium-dependent manner, and enhanced in activated microglia by the p38 MAPK pathway that selectively regulates slowly mobile receptors. Thus, our data indicate that P2X4 receptors are dynamically regulated mobile ATP sensors, sampling more of the plasma membrane in response to ATP and during the activated state of microglia that is associated with nervous system dysfunction.

Microglia are resident immune cells of the brain and are involved in a variety of nervous system disorders (1, 2). They represent about 10% of the cells in the central nervous system and usually exist in a resting physiological state but enter activated states during injury and disease settings (1, 3). The activated states of microglia display altered physiological responses and are known to contribute to nervous system dysfunction through interactions with neurons and astrocytes (1, 3, 4).

ATP, a neuro- and gliotransmitter (5), activates P2X receptors that are trimeric ATP-gated cation channels comprising seven homomeric receptors (P2X1 to P2X7) and several heteromeric assemblies (6, 7). The most widely expressed P2X subunits in microglia are P2X4 and P2X7, which form homomeric receptors and undergo functional interactions (8, 9). Important roles for P2X4 receptors in microglial function are demonstrated by experiments showing that microglia are involved in the development of neuropathic pain (4, 10–13). Strategies that reduce microglial P2X4 receptor function alleviate symptoms in neuropathic pain models, demonstrating that altered P2X4 receptor function in activated microglia is a critical step in the development of this disorder (10–13). Consequently, P2X4 receptors are major drug targets to treat pain states that are currently resistant to therapy (4, 14). In view of these roles, considerable effort has been devoted to studying P2X4 receptors. Of most relevance here, P2X4 receptors are known to display high calcium permeability (15, 16) and undergo dynamic trafficking onto and off the plasma membrane (17–25).

Regulation of receptor lateral mobility in the plasma membrane is a recently discovered cell surface trafficking mechanism with roles in calcium-dependent regulation of synaptic strength (26–30). Thus, quantum dot (QD)[3]-based single-molecule imaging and single particle tracking (SPT) have shed light on the regulation of several neurotransmitter receptors, including P2X2 receptors (26, 31, 32), which are known to display different types of lateral mobility in the plasma membrane with proposed and demonstrated signaling roles (26). In contrast, the lateral mobility of P2X4 receptors has not been measured, and little is known about this aspect of their function or even if mobility is regulated by ATP or in settings where P2X receptors are known to play critical roles, such as in resting and activated microglia.

EXPERIMENTAL PROCEDURES

Molecular Biology—An overlapping PCR method was used to introduce an HA tag (YPYDVPDYA) at position Gln-78 of rat P2X4 or P2X4-YFP to generate $P2X4^{HA}$ and $P2X4^{HA}$-YFP, respectively. The resulting PCR product was subcloned into pcDNA3.1 using HindIII and XhoI restriction sites. $P2X2^{FLAG}$ was made in the same way following past detailed characterization work by others (32–34), and its properties have been described fully (32). P2X4 K67A and P2X4 Y378A point mutations were generated using rat $P2X4^{HA}$ or P2X4-YFP as a template using QuikChange mutagenesis (Stratagene). cDNAs

* This work was supported, in whole or in part, by National Institutes of Health Grant NS073980. This work was also supported by an award from Johnson & Johnson, a Stein-Oppenheimer Foundation Endowment Award, and unrestricted funds from UCLA (to B. S. K.).

[1] Present address: Institut des Maladies Neurodegeneratives, CNRS UMR 5293, 146, Rue Leo Saignat, 33076 Bordeaux Cedex, France.
[2] To whom correspondence should be addressed. E-mail: bkhakh@mednet.ucla.edu.

[3] The abbreviations used are: QD, quantum dot; *D*, diffusion coefficient; SPT, single particle tracking; FRAP, fluorescence recovery after photobleaching; MSD, mean square displacement; PSF, point-spread-function; pF, picofarad; BAPTA, 1,2-bis(2-aminophenoxy)ethane-*N*,*N*,*N*′,*N*′-tetraacetic acid.

were propagated in DH5α *Escherichia coli,* and plasmids were purified using standard techniques. All constructs were verified by sequencing. P2X4-YFP receptors were available from our past work, and the C-terminal YFP/GFP/cyan fluorescent protein tags have been extensively characterized in P2X4 receptors and shown not to alter receptor properties (17, 21, 35, 36).

HEK-293 Cell Culture and Transfection—HEK-293 cells (ATCC) were maintained in 75-cm^2 cell culture flasks in Dulbecco's modified Eagle's medium/F-12 media with Glutamax (Invitrogen) supplemented with 10% fetal bovine serum and 1% penicillin/streptomycin. Cells were prepared for transfection by plating onto 6-well plates at the time of splitting, 3–4 days before transfection. They were transfected at ~60% confluence. For transient expression in HEK-293, we used ~0.5 μg of plasmid and the Effectene transfection reagent (Qiagen). When appropriate, 100 ng of YFP was used as a marker of transfected cells. The manufacturer's instructions (Qiagen) were followed. Cells were gently dispersed and plated on poly-D-lysine-coated glass coverslips (12 mm diameter).

C8-B4 Microglial Cell Culture and Nucleofection—The mouse immortalized microglial C8-B4 cell line was characterized previously (25, 37, 38). The cells were cultured in 25-cm^2 cell culture flasks in Dulbecco's modified Eagle's medium (ATCC) supplemented with 10% fetal bovine serum (ATCC). The cells were split 1 in 3 when confluence reached ~60%. C8-B4 microglia cells were transfected by Amaxa nucleofection with 3–4 μg of plasmid DNA before plating onto polylysine-coated glass coverslips. The manufacturer's instructions were followed using the Amaxa basic nucleofection kit for mouse astrocytes. We transfected C8-B4 microglia with plasmids using nucleofection (rather than transfection) as this preserved the cells in the resting state and allowed us to trigger the activated state when required by exposure to inflammatory mediators (see under "Results"). Thus 100 μM ATP-evoked currents in control C8-B4 cells, and those expressing YFP via nucleofection were negligible at -0.3 ± 0.2 and -0.4 ± 0.1 pA/pF ($n = 6$), as expected for resting microglia (25). In comparison, microglia activated with LPS (3 h, 1 mg/ml) displayed ATP-evoked currents of -8.8 ± 2.5 pA/pF ($n = 19$), as reported previously (25). These data indicate that the act of gene expression by nucleofection does not trigger microglia to enter the activated state. Cells were recorded and imaged 24–48 h after transfection.

Whole-cell Patch Clamp Recording—For microglia the extracellular recording solution included the following (in mM): NaCl (130), KCl (3), $MgCl_2$ (1), $CaCl_2$ (2), HEPES (10), and glucose (10), and the pipette solution contained KCl (130), $MgCl_2$ (2), $CaCl_2$ (0.5), EGTA (5), and HEPES (10). To test the role of Ca^{2+}, we either omitted $CaCl_2$ in the bathing solution and added 5 mM EGTA or included 3 mM BAPTA in the patch pipette solution, as indicated in the text. For the ionomycin experiments, we used 8 mM $CaCl_2$ in the extracellular buffer. The methods for HEK-293 cells were similar as those for microglia except that they were used within 48 h of transfection. The HEK-293 cell extracellular recording solution included the following (in mM): NaCl (147), KCl (2), $MgCl_2$ (1), $CaCl_2$ (1), HEPES (10), and glucose (10) with a pH adjusted at 7.4 with NaOH. The pipette solution contained KCl (154), EGTA (11), and HEPES (10). Whole-cell voltage clamp recordings were made using ~4 megohm glass borosilicate electrodes (World Precision Instruments) with an Axopatch 200B or 700A amplifier controlled by computers running pCLAMP8.1 software via a Digidata 1322A interface (Axon Instruments). Data were filtered at 2 kHz and digitized at >5 kHz.

QD Labeling and Imaging of Microglia—We used QDs to study P2X4 receptor mobility using procedures that are essentially identical to those we recently reported for P2X2 receptors (32). QDs are fluorescent nanometer sized semiconductor crystals with narrow emission spectra (39). They are excellent fluorescent probes for single-molecule imaging as they are brighter than organic fluorophores and undergo less bleaching (26, 30, 39).

Microglial cells were used 24–48 h after transfection with $P2X4^{HA}$ plasmids. Fluorescence was captured using an Olympus IX71 microscope with a ×60 1.45 NA Olympus objective lens and an EMCCD camera (Andor Ixon DV886JCS-VP). This camera has a chip pixel size of 8 × 8 μm, which means the effective image pixel size with a ×60 lens is 130 × 130 nm, equivalent to an area of 0.017 μm^2. Excitation was provided by a Polychrome V monochromator (TILLVision). Appropriate filters (Chroma Technology) were chosen for YFP and QDs emitting 655 nm light. Imaging media used for all experiments were the same as the electrophysiology recording media. The cells were continually perfused. ATP (Sigma) was applied using a fast solution switcher (VC-77SP Fast-Step Perfusion System; Warner Instruments). Ca^{2+}-free solutions were applied 2 min before and during the ATP application. Incubation with LPS (Sigma; 1 μg/ml, 4 h), minocycline (Sigma; 200 μg/ml, 1 h preincubation), SB203580 (Sigma; 10 μM, 1 h preincubation), and poly(I:C) (Sigma; 50 μg/ml, 3 h) was made in complete cell media at 37 °C. The LPS we used was from *E. coli* 055:B5 (order number L2880 from Sigma). Incubation with fibronectin (Invitrogen; 10 μg/ml, 30 min) and dynasore (Ascent; 80 μg/ml, 45 mins) were made in recording media at 37 °C. Labeling of $P2X4^{HA}$ and $P2X2^{FLAG}$ receptors with QDs was performed using mouse biotinylated anti-HA antibodies (Santa Cruz Biotechnology, Santa Cruz, CA) and mouse biotinylated anti-FLAG antibodies (Invitrogen), respectively, followed by streptavidin-conjugated QD655 (Invitrogen). Labeling was performed at room temperature in 1 ml of solution. Incubation of primary antibody (10 μg/ml) was for 20 min, and QD incubation (5 pM) was for 5 min (in recording media).

Intracellular Calcium Ion Imaging—Microglial cells were loaded with 2.5 μM FURA2-AM (Invitrogen) in the presence of pluronic acid (0.05%) in the extracellular buffer for 15 min and then transferred to a dye-free buffer for 15 min before experimentation to allow cleavage of the AM ester group. For the "zero" extracellular Ca^{2+} experiments, prior to the experimentation, cells were incubated for 2 min in a bath solution containing no added calcium and supplemented with 5 mM EGTA. The cells were viewed with a ×40 oil immersion objective lens with a numerical aperture of 0.8 (Olympus).

Fluorescence Recovery after Photobleaching (FRAP)—FRAP and confocal microscopy were carried out using an Olympus BX61WI and FV300 Fluoview laser scanning confocal microscope using a 488 nm argon laser, a ×40 objective lens with an

NA of 0.8, and Fluoview software. Bleaching was achieved in a 2-μm^2 area with 100% laser power for ~1 s, followed by examination of recovery over 30 s at 3 frames/s (with the laser power at 0.1% of maximum).

Single Particle Tracking and Data Analysis—We used methods described previously (32). Briefly, for analysis of QD-labeled receptor mobility, images were acquired every 100 ms for a duration up to 60 s, but note that data were analyzed over observation periods ranging from 0.5 to 30 s as described below and in the results. Trajectories of receptor mobility were generated using single particle tracking methods implemented into an analysis package called AsteriX written in National Instruments LabVIEW, as recently described (40, 41). The software allows for fitting of individual point-spread-functions (PSFs) with a two-dimensional Gaussian profile within selected circular regions of interest. A semiautomatic fitting process repeats this frame-after-frame, centering on the regions of interest of the previously fitted PSF position. The quality of the fit can be checked manually on a frame by frame basis. Single QDs were identified by their fluorescence blinking. Because of random blinking events, the trajectory of an individual receptor could not always be tracked continuously. During QD blinking periods, no fit was attempted. The center of each fitted position was then connected by straight lines to represent the QD trajectory. For each fitted PSF, the integrated intensity within a selectable numbers of pixels centered on the PSF (usually 3×3 pixels) was represented as an intensity time trace, allowing the visualization of "on" and "off" emission periods (*e.g.* Fig. 3*B*). Tracking was aborted when a PSF did not reappear within 5 s. Tracking was also aborted when two QD-labeled $P2X4^{HA}$ receptors crossed paths. Analysis of QD diffusion was performed using two different approaches as follows: (i) the diffusion coefficient (D) for trajectories was estimated using the mean square displacement curve (MSD), and (ii) the instantaneous diffusion coefficient (D_{app}) was estimated over time. Thus D was estimated from analysis of the MSD curve over the first 10% of the plot that covered track segments of 300 frames in length (*i.e.* 30 frames were used for MSD analysis, which corresponds to an observation time of 3 s). In some cases we used an observation time of 30 s (see "Results"). D_{app} was estimated from smaller MSD plots calculated over contiguous trajectory stretches of five frames (*i.e.* an observation time of ~0.5 s). This allowed us to obtain a running measure of D_{app} over time before and during fast ATP applications and simultaneous whole-cell patch clamp recordings. For these experiments, note that in the results we verified measurements of ATP-evoked changes in D_{app} by also performing analysis of D over longer observation periods (30 s). Thus, no analysis of D was made with an observation time of 100 ms, which was the frame rate. In most cases we performed simultaneous patch clamp and SPT, but in some instances we performed SPT without simultaneous patch clamp. The results did not differ using these approaches, and the data have been pooled (total of 66 cells; Table 2), as recently shown for our studies for P2X2 receptors where we compared patched and nonpatched cells (32). As described under "Results," most P2X4 receptors displayed linear MSD plots that were fit as shown in Equation 1,

$$\langle r^2 \rangle = 4e^2 + 4Dt \qquad \text{(Eq. 1)}$$

where the slope is $4D$ and the error is e (Fig. 4). In the MSD-time interval plot in Fig. 4, D is 0.036 $\mu m^2/s$ and e is ~141 nm, of which a component is due to diffusive blurring during acquisition. We observed that ~11% of P2X4 receptors displayed flat MSD plots indicative of corralled diffusion that were fit with Equation 2,

$$\langle r^2 \rangle \cong 4e^2 + R^2\{1 - A_1 \exp(-4A_2Dt/R^2\} \qquad \text{(Eq. 2)}$$

where R is the corral size and A_1 and A_2 are theoretical constants for a lattice of square corralling regions (42).

Software and Statistical Analysis—SPT was performed with AsteriX running in National Instruments LabVIEW (40, 41). All electrophysiology data analysis was performed with Clampfit 10.1 (Molecular Devices Axon Instruments), Origin 7.5 or 8.1 Pro (OriginLab Corp.), GraphPad Instat 3.0 (GraphPad Software), or ImageJ (National Institutes of Health). Data are as mean ± S.E. from at least five experiments.

RESULTS

In this study, we used C8-B4 microglial cells (herein called microglia) for four reasons. First, like microglia *in vivo* they normally exist in the resting state but can be made to enter an activated state that recalls several aspects of P2X4 receptor regulation in disease (25, 38). Although the activated states of microglia *in vivo* are likely to represent a spectrum of states, in this study we used the generalized term "activated" to signify C8-B4 cells after treatment with LPS or fibronectin. Both of these strategies cause molecular alterations in C8-B4 microglia that are indicative of activated microglia (25, 38). Conversely, we used the term "resting" to signify microglia that had not been challenged by LPS or fibronectin. Second, C8-B4 cells natively express P2X4 receptors that display functional properties as expected of molecularly defined P2X4 receptors *in vitro* and *in vivo* (25, 43). Third, C8-B4 microglia up-regulate expression of P2X4 receptors in the plasma membrane (and also markers of activated states) when they are challenged with LPS or fibronectin, which is reminiscent of P2X4 up-regulation within microglia *in vivo* (25). Fourth, our work shows that only homomeric P2X4 receptors are expressed within C8-B4 cells (25). For all these reasons, C8-B4 cells are an ideal model cell to study P2X4 mobility in a native-like environment. In addition, one should note that single-molecule imaging can currently only be performed in cultured cells because of their favorable optical properties.

Initial Observations with Fluorescence Recovery after Photobleaching (FRAP)—We began our experiments with FRAP and start by providing reasons why we did this. First, recent work with P2X1 receptors carrying fluorescent protein tags suggests that FRAP can be used to study receptor trafficking and mobility (44, 45). In light of these data, we used previously characterized YFP-tagged P2X4 receptors (P2X4-YFP) and FRAP to study receptor trafficking and macroscopic mobility (17, 35, 36, 46). Second, FRAP is a relatively simple method, and our hope was we could also use this in our studies of P2X4 receptor trafficking. As reported below, our data show FRAP cannot be used

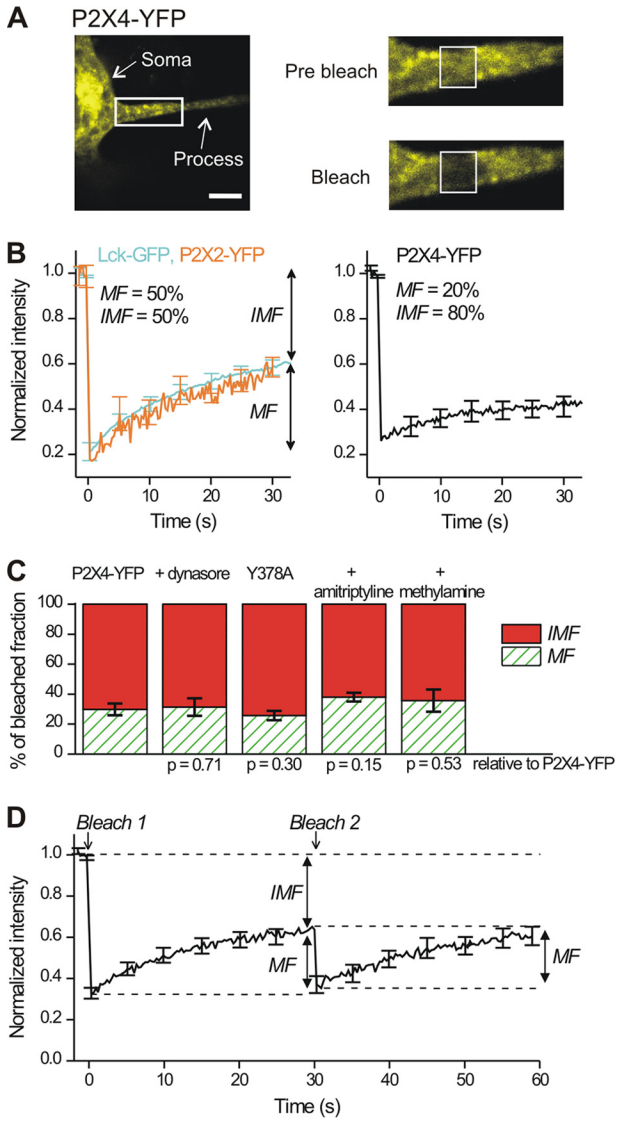

FIGURE 1. **Macroscopic FRAP studies of P2X4-YFP receptor mobility.** *A* shows an image of a microglial process expressing P2X4-YFP receptors. The *boxed region* is enlarged in the images to the *right*, both before and immediately after a period of photobleaching indicated by the *boxed areas*. *B, left-hand* FRAP curves are for membrane-targeted GFP (Lck-GFP) and P2X2-YFP receptors expressed in microglia. The *right-hand* FRAP curve is for P2X4-YFP receptors expressed in microglia. *C, bar graphs* show the proportion of mobile and immobile fractions for P2X4-YFP receptors under control settings (n = 20) and under the various conditions indicated, which are when the cells were incubated with dynasore (80 μM; n = 11), amitriptyline (50 μM; n = 12), or methylamine (50 mM; n = 7) and when the microglia expressed P2X4-YFP receptors carrying the Y378A mutation in the known endocytic motif (n = 14). The p values show the results of statistical comparisons between the indicated data sets and control; there were no differences. There was no significant difference between the mobile and immobile fractions relative to control. *D, graph* shows average FRAP data for microglial processes when the same region was bleached twice ~30 s apart (n = 20).

reliably in this regard, and we present these negative data to serve as a guide for future studies of P2X4 receptor trafficking.

We measured FRAP for P2X4-YFP in microglia and used P2X2-YFP and membrane-targeted GFP (Lck-GFP) for comparison (32, 47, 48). We found that the mobile fraction of P2X4-YFP receptors at ~20% was smaller than for P2X2-YFP or Lck-GFP (~50%; Fig. 1, *A* and *B*). Conversely, the P2X4-YFP immobile fraction was larger. In some cases FRAP mobile and immobile fractions can reflect insertion and/or removal of membrane receptors (46). However, the size of the P2X4-YFP receptor mobile fraction was not significantly altered in cells treated with dynasore (Fig. 1*C*, 80 μM) or for P2X4-YFP receptors carrying Y378A mutations, both of which are known to block P2X4 endocytosis (20, 21, 25). Moreover, the mobile fraction was unaltered in cells treated with amitriptyline (50 μM) and methylamine (50 mM), which reduce and increase lysosomal secretion of P2X4 receptors, respectively (20, 25). For all these comparisons, the results of statistical comparisons with control P2X4-YFP receptors are presented in Fig. 1*C*. We also performed two consecutive rounds of FRAP in single ~2-μm^2 areas. We reasoned that if significant membrane receptor exchange occurs from an intracellular pool, then a second round of FRAP should reveal immobile and mobile fractions. If, however, detectable trafficking does not occur, then a second round of FRAP should only reveal a mobile fraction, as the immobile receptors would have been bleached in the first round. We found that a second round of FRAP revealed only a mobile fraction (Fig. 1*D*).

In contrast to recent FRAP work with P2X1 receptors (44, 45), our FRAP data show that the P2X4-YFP receptor immobile fraction does not reflect detectable turnover. This suggested that the immobile pool may represent distinct types of plasma membrane lateral diffusion and/or an intracellular pool. FRAP cannot discriminate between these possibilities leading us to explore single-molecule imaging, which is one of the few available methods that can (26). Overall, our data show that FRAP is not a very useful method to study P2X4-YFP receptor mobility or trafficking under the conditions we have examined, but of course this does not detract from past studies on P2X1 receptors in HEK-293 cells as they may display more extensive trafficking over the relevant time scales (44, 45).

Engineered P2X4^{HA} Receptors for Single-molecule Imaging—There are no antibodies available against the extracellular domain of P2X4 receptors. We thus engineered P2X4 receptors to carry HA epitope tags (P2X4^{HA}) in the extracellular domain at Gln-78 and transfected them into microglia (Fig. 2), which express very few native plasma membrane P2X4 receptors in the resting state (25). We chose this site because tag insertion at the equivalent position in P2X2 receptors is innocuous (32–34) and because this site is surface-exposed (Fig. 2*A*) (49). In accord, we found that ATP sensitivity, current waveforms (Fig. 2*B*), and peak current densities were not significantly different for wild type (WT) P2X4, P2X4^{HA}, and P2X4^{HA} receptors labeled with amounts of QDs that are expected to result in near complete labeling based on our past experiences (32), although it is impossible to be absolutely sure that receptors were labeled to saturation. In Fig. 2*B*, 100 μM ATP-evoked currents were -80 ± 8, -77 ± 5, and -72 ± 5 pA/pF, respectively (n = 8, 6, and 6). Cell surface P2X4^{HA} receptors could also be labeled with biotinylated anti-HA antibodies and streptavidin-coated QDs (Fig. 2*C*). We next modified P2X4-YFP receptors to carry HA at Gln-78 (P2X4^{HA}-YFP) and assessed their macroscopic mobility using FRAP before and after QD labeling (see below for dose-response analysis of P2X4^{HA}-YFP receptors). We found that QD labeling did not alter FRAP (Fig. 2*D*). These data show that an HA tag at Gln-78 of P2X4 (Fig. 2*A*) is accessible to QDs (Fig.

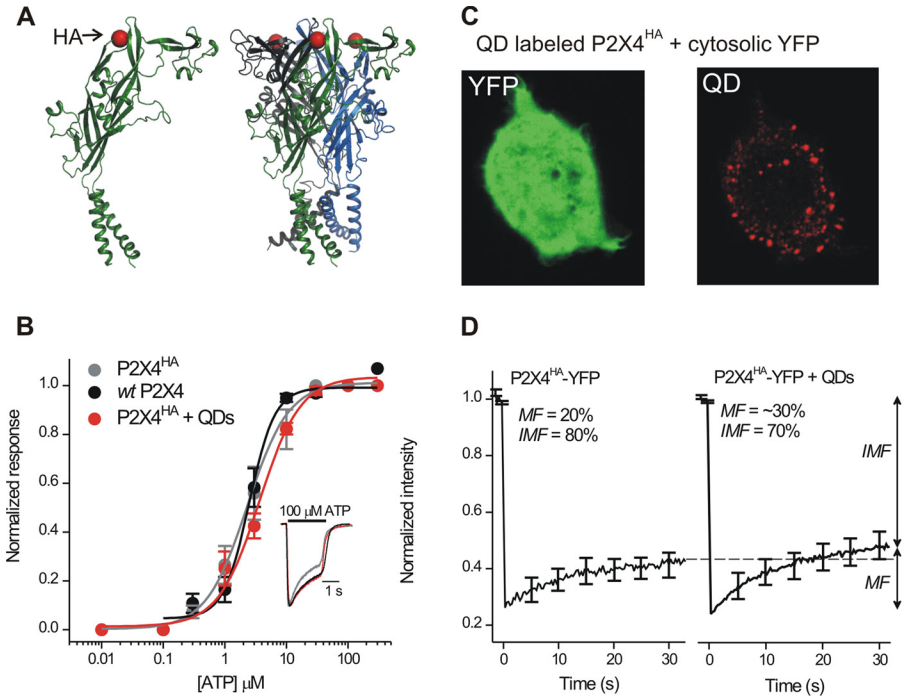

FIGURE 2. **HA tag at Gln-78 in P2X4^{HA} receptors is surface-exposed and can be labeled with QDs without altering receptor function or macroscopic mobility.** *A,* models show a single P2X4 subunit (*left*) and a trimeric P2X4 receptor (*right*) with the HA tag insertion site shown schematically as a *red ball* (at Gln-78) in the extracellular domain. *B,* normalized concentration-effect curves for ATP at WT P2X4, P2X4^{HA}, and P2X4^{HA} receptors transfected into microglia and labeled with 100 pM QDs to ensure that most receptors were bound to QDs (n = 8, 6, and 6). The *inset* shows normalized representative 100 μM ATP-evoked currents from the three concentration-effect curves. *C,* representative image of a HEK cell expressing P2X4^{HA} receptors and cytosolic YFP. The QD image was obtained using a high amount of QDs (100 pM) to ensure most surface receptors were labeled. *D,* FRAP curves for P2X4^{HA}-YFP receptors with (n = 20) and without QD labeling (n = 12). There was no decrease in the mobile fraction (*MF*) from FRAP recovery curves. If anything, there was a small trend for the mobile fraction to be greater after QD labeling (36 ± 3 *versus* 22 ± 3% for P2X4^{HA}-YFP and P2X4^{HA}-YFP + QD receptors, respectively; $p < 0.01$ with an unpaired Student's t test). Overall, these data indicate that QD labeling did not decrease P2X4 receptor mobility.

2*C*) and that neither the tag nor the QDs detectably alter receptor function (Fig. 2, *B* and *D*).

Imaging Single QD-labeled P2X4^{HA} Receptors in Microglia—Microglia expressing P2X4^{HA} plus cytosolic YFP were labeled with red QDs (5 pM; Fig. 3*A*) revealing about five P2X4^{HA} receptors per cell (Fig. 3*A*). No such labeling was observed in microglia expressing YFP alone or when the primary antibody was omitted. We counted QD-labeled P2X4 receptors in parallel with patch clamp analysis of 100 μM ATP-evoked currents (−9 ± 1 pA/pF for microglia with capacitances of 46 ± 2 pF; n = 15), and we estimated that ~1–2% of the surface receptors (50) were labeled with QDs. The QD-labeled P2X4 receptors on microglia displayed "blinking" characteristic of single molecules (Fig. 3*B*), and their intensity in microglia was identical to single QDs in solution (Fig. 3*C*) allowing us to easily identify and image single QD-labeled P2X4^{HA} receptors (Fig. 3, *B–D*).

Distinct Types of P2X4 Receptor Lateral Mobility in Microglial Processes—We used SPT and mean square displacement (MSD) analysis to measure diffusion coefficients (D) for QD-labeled P2X4^{HA} receptors in microglial processes. The experiments reported in this study were for processes that were 40 ± 3 μm long, 6 ± 0.4 μm thick, and with the QD-labeled receptors typically located 18 ± 1 μm from the soma, although we studied all receptors along processes independent of their location (distance measurements are for 90 receptors from 17 cells but are representative of >1800 receptors studied over 1 year). We chose to analyze receptors on processes rather than the soma because they were relatively flat, and the soma was round. Also, the soma often contained blobs of intracellular P2X4 receptor expression (measured using P2X4-YFP; see below), which was not observed in the processes.

A plot of MSD against time interval t takes three forms (26, 51). First, the MSD *versus* t plot may be linear, defining Brownian motion. Second, the plot may tend to a constant value representing corralled/restricted diffusion. Third, the plot may be steep, representing directed motion (51). From a specific set of experiments, we found that 88% of P2X4^{HA} receptors in microglia displayed linear MSD plots, whereas ~10% displayed flat MSD plots indicative of corralled diffusion (Fig. 4, *A* and *B*; Table 1) with a corral size of 0.04 ± 0.01 μm^2 (n = 32 trajectories; see under "Single Particle Tracking and Data Analysis" and Table 1). For subsequent studies, we measured the mean values for D for the corralled and linear trajectories as well as their proportions and present these values in Table 1. In the sections below, we focused on the majority of trajectories that were linear because these displayed significant changes depending on the resting/activated status of microglia. However, we observed no marked or consistent change in the small proportion (~12% across all experiments) of corralled trajectories under different conditions (Table 1).

The example linear MSD plot in Fig. 4*C* represented a trajectory that covered an area of 3.45 μm^2 in 30 s with D = 0.036 μm^2/s. We repeated this analysis for all linear MSD plots (n = 258) for single P2X4 receptors and found a bimodal histogram representing two classes of D in the processes of resting microglia (Fig. 4*E*). Note that in Fig. 4*E* the x axis is on a log scale,

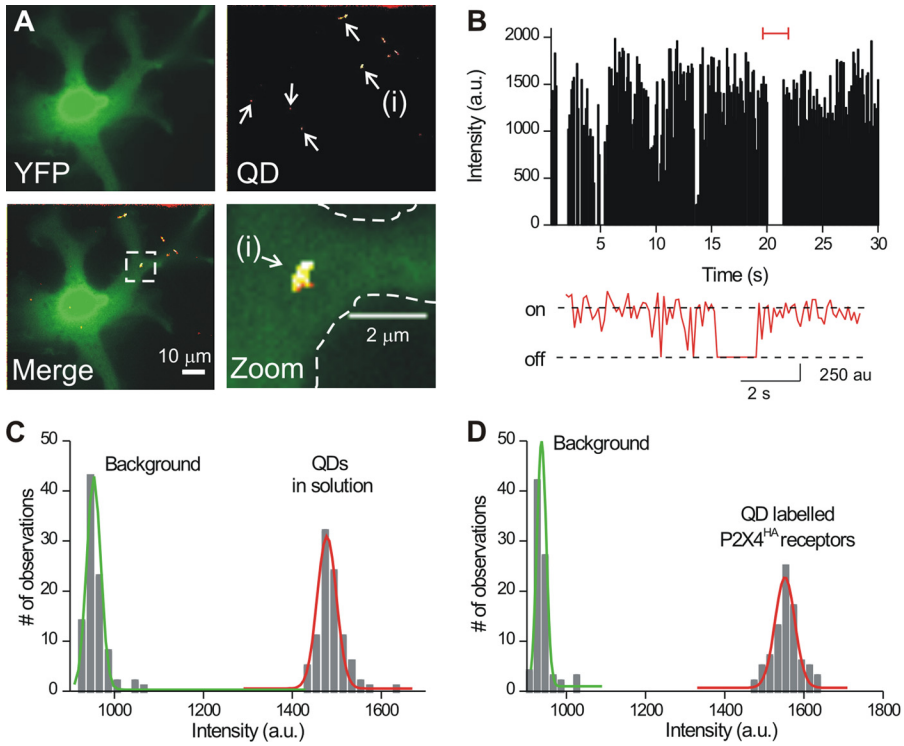

FIGURE 3. **Imaging single plasma membrane P2X4^{HA} receptors labeled with QDs.** *A* show images of a microglial cell expressing P2X4^{HA} receptors and cytosolic YFP. The YFP image (*upper left panel*) reveals the shape of the cell whereas the QD image shows several spots of fluorescence (indicated by *arrows*). This is more readily seen in the merged image at the *lower left*. The *boxed region* for this image has also been enlarged. *B, graph* shows the intensity of a QD-labeled P2X4^{HA} receptor plotted over time, revealing two overall states that correspond to when the QD is fluorescent and when it is not. *C, graph* shows the intensity of single QDs in relation to background noise when the dilute QDs were imaged in buffer. *D, graph* shows a similar plot to that in *C* in relation to background, but in this case the QD intensities are taken from single frames from images such as those in *A*, where P2X4^{HA} receptors were labeled with QDs.

indicating and accurately showing a broad spread of values for *D*. We could not describe this distribution with a single Gaussian peak and hence used a double Gaussian function, which was the simplest fit that described the data. From the *graph* in Fig. 4*E*, it is also clear that a few trajectories have a very low value of *D* (between −6 and −8 on the *x* axis). We emphasize that our data fall short of adequately analyzing these because their numbers were too low to systematically study. Thus, it remains possible that a third very slow mobility peak exists in the P2X4^{HA} trajectory characteristics, something that would be worth exploring in future studies. Henceforth, we termed receptors as "slowly mobile" if *D* differed by more than three standard deviations from the center of the largest peak representing the fastest pool, which we termed the "mobile pool" (Fig. 4*E*). The mean value of *D* for mobile receptors was 0.023 ± 0.001 $\mu m^2/s$ ($n = 210$; Table 1) representing 66% of all receptors. The slowly mobile P2X4^{HA} receptors displayed a *D* value that was ~20 times lower than the mobile pool (0.001 ± 0.0004 $\mu m^2/s$; $n = 77$) representing 24% of all receptors. The differences in membrane explored is readily apparent from the trajectory areas, which were 1.4 ± 0.1 ($n = 210$) and 0.2 ± 0.04 μm^2 ($n = 77$) for mobile and slowly mobile receptors, respectively.

Slowly Mobile Receptors May Not Reflect Receptor Clusters—Would individual slowly mobile QD-labeled P2X4^{HA} receptors reflect the location within P2X4 receptor clusters that were unlabeled with QDs? To address this, we used P2X4^{HA}-YFP and QD-labeled P2X4^{HA}-YFP receptors. These receptors functioned like WT P2X4 in terms of ATP sensitivity (Fig. 5, *A* and *B*), current waveforms, and peak responses, which for a specific set of comparative experiments were −46 ± 9, −51 ± 9, and −35 ± 6 pA/pF ($n = 5$, 6, and 6; 100 μM ATP) for WT P2X4, P2X4^{HA}-YFP, and QD-labeled P2X4^{HA}-YFP receptors, respectively. We found that the mobility of single QD-labeled P2X4^{HA}-YFP receptors was not related to the YFP intensity of the underlying trajectory (Fig. 5*C*) arguing against any obviously detectable role of receptor clustering in contributing to mobility. When interpreting this experiment, it is important to consider several points associated with this type of analysis. First, the measurement of YFP intensity is diffraction-limited, meaning it is not possible to rule out cytosolic fluorescence. However, when performing this analysis, we focused on QDs that were located in processes (as in other parts of this study, see *arrow* in Fig. 5*B*), and this avoided the large blobs of fluorescence often seen in the soma (Fig. 5*B*). We also examined slowly mobile QD-labeled P2X4^{HA}-YFP receptors directly and found that the YFP intensity of the underlying trajectory was no different from that of nearest regions (at 1296 ± 423 and 954 ± 169 arbitrary units of fluorescence intensity, respectively; $p > 0.05$, $n = 56$). Thus, within the limits of the resolution of light microscopy, we found no evidence to suggest that slowly mobile P2X4^{HA}-YFP receptors represented clusters. However, it remains formally possible that similar levels of YFP fluorescence may reflect different levels of surface receptors, an issue that will require further developments in light microscopy to address.

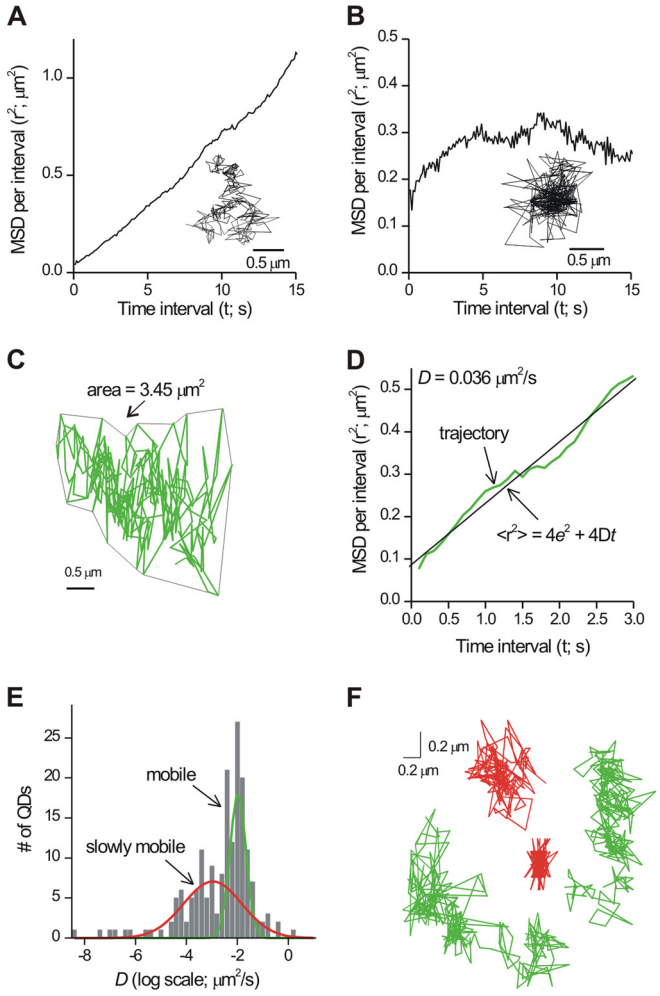

FIGURE 4. **Lateral mobility of single P2X4^{HA} receptors in the plasma membrane of resting microglial cells.** *A* and *B* show representative trajectories extracted from single QD movies (300 frames) along with their associated graphs of MSD against time interval *t*. P2X4^{HA} receptors displayed two types of MSD plots, linear MSD plots as illustrated in *A* or corralled MSD plots as illustrated in *B*. Both are described in detail in the text. *C*, representative trajectory for P2X4^{HA} receptor mobility in resting C8-B4 microglia. *D, graph* shows the MSD plot for the trajectory shown in *C*. This was best fit with the equation shown, from which the estimate of the diffusion coefficient *D* was obtained. *E, histogram* showing two pools of membrane P2X4^{HA} receptors with separable values of *D*. We called these mobile (for the high *D*) and slowly mobile if the value for *D* differed by more than three standard deviations from the mean of the mobile pool. *F* shows representative trajectories for two mobile (*green*) and two slowly mobile (*red*) P2X4^{HA} receptors in microglia.

Use-dependent Regulation of P2X4^{HA} Receptor Lateral Mobility in Resting Microglia—We combined single-molecule imaging with fast ATP applications to determine whether P2X4 receptor mobility was changed by receptor activation (Fig. 6*A*). In all cases, we measured ATP-evoked currents from the microglia, and in most cases this was done with simultaneous patch clamp and SPT. We analyzed P2X4 receptor mobility by plotting the diffusion coefficient from 0.5-s trajectory tracts and plotted it on the same time scale as ATP-evoked whole-cell currents (Fig. 6, *B* and *C*). Because the trajectory tracts for this analysis were short (in order to follow over time), we could not reliably distinguish trajectory subclasses as shown in Table 1 because this requires longer periods of analysis (typically ~30 s). For this reason, we termed the running measure of *D* from short tracts as D_{app} as this value represents an apparent diffusion coefficient (D_{app} does not distinguish between mobile and slowly mobile receptors described above and in Table 1).

For a specific set of experiments, the 100 μM ATP-evoked currents were −10 ± 1 pA/pF, and the value for D_{app} changed from ~0.02 ± 0.002 μm²/s to 0.04 ± 0.004 μm²/s (n = 17 cells, 90 receptors; Fig. 6*C*). The 10–90% rise time of the ATP-evoked current was 157 ± 21 ms, whereas the rise time of the change in D_{app} was significantly slower at 1.5 ± 0.2 s ($p < 0.05$). As expected, the increase in P2X4 receptor mobility increased the area of the membrane that was sampled from 0.43 ± 0.05 to 1.13 ± 0.17 μm² (n = 90). Moreover, as the P2X4 receptor current desensitized, the increased mobility returned the pre-ATP levels (Fig. 6*C*).

We performed an additional level of analysis to make sure that ATP applications did in fact change P2X4^{HA} mobility and that the changes in D_{app} were not misleading. Thus, we performed full trajectory analysis (as in Fig. 4) for 30 s before ATP and for 30 s during ATP. The data shown in Fig. 6*D* clearly show that *D* for P2X4^{HA} receptors is increased in the presence of ATP. Thus, our finding that ATP increases P2X4^{HA} mobility is based on analysis of D_{app} on the seconds time scale and using analysis of *D* on the tens of seconds time scale (Fig. 6, *C* and *D*). Taken together, these data provide strong evidence that ATP increases P2X4^{HA} mobility.

Use-dependent Regulation of P2X4^{HA} Receptor Lateral Mobility Is Triggered by Cytosolic Calcium Elevations and Is Abolished in Activated Microglia—We explored mechanisms underlying how P2X4 receptor mobility is regulated by ATP by investigating the role of calcium entry, which is known to affect the mobility of other receptors (26). We thus repeated the experiments shown in Fig. 6*C* with extracellular buffers lacking calcium and found that the ATP-evoked increase in mobility was abolished, but the ATP-evoked currents were normal (Fig. 7*A*). A similar result was obtained when the cells were dialyzed with 3 mM BAPTA to chelate intracellular calcium (Fig. 7*B*; Table 2). In a separate series of experiments, we estimated the change in calcium concentration triggered by ATP (Table 3). Resting cytosolic calcium levels were ~100 nM within microglia but increased to 490 ± 15 nM 2 s after applying 100 μM ATP (n = 9), *i.e.* when the increase in P2X4 receptor mobility reached its peak (*arrow* in Fig. 6*C*). The change in calcium levels peaked at ~1 μM (Table 3).

We exploited previously reported "dead" P2X4^{HA}K67A receptors that are defective in binding ATP but are surface-expressed (32, 47, 52–54). Patch clamp and SPT revealed negligible ATP-evoked currents, and no ATP-evoked changes in mobility of P2X4^{HA}K67A receptors (Fig. 7*C*), indicating that binding of ATP to P2X4 receptors is required for the ATP-evoked increase in mobility. This control experiment also dismisses nonspecific effects of ATP applications on microglia.

Next, we addressed whether P2X4 receptor mobility increases that were calcium-dependent (Fig. 7) required calcium flux via P2X4 receptors or if they could be triggered by elevating cytosolic calcium by other means. We thus imaged QD-labeled P2X4^{HA} receptors and applied the calcium-selective ionophore ionomycin (5 μM; Fig. 7*D*). To our surprise, we found that ionomycin caused a significant increase in D_{app} for P2X4^{HA} receptors from 0.02 ± 0.003 to 0.05 ± 0.005 μm²/s

TABLE 1
Basal $P2X4^{HA}$ and $P2X2^{FLAG}$ receptor mobility

	No. of QDs	Corralled D ($\mu m^2/s$) means ± S.E. (proportion; %) (S.D.)	Linear mobile D ($\mu m^2/s$) means ± S.E. (proportion; %) (S.D.)	Linear slowly mobile D ($\times 10^{-4}$ $\mu m^2/s$) means ± S.E. (proportion; %) (S.D.)	p^a
Studies with $P2X4^{HA}$ in microglia					
Control	319	0.008 ± 0.001 (10) (0.01)	0.023 ± 0.001 (66) (0.041)	9.2 ± 3.3 (24) (3.3)	<0.01
+ LPS[b]	155	0.01 ± 0.003 (9) (0.01)	0.016 ± 0.001 (85) (0.015)	4.1 ± 1.0 (6) (2.9)	<0.01
+ fibronectin[b]	68	0.017 ± 0.008 (10) (0.02)	0.012 ± 0.002 (85) (0.011)	5.0 ± 0.7 (4) (1.2)	<0.01
+ LPS + minocycline	120	0.009 ± 0.004 (9) (0.014)	0.014 ± 0.001 (72) (0.012)	2.6 ± 0.7 (19) (3.2)	<0.01
+ LPS + SB203580	130	0.007 ± 0.002 (16) (0.007)	0.011 ± 0.002 (59) (0.013)	4.6 ± 0.6 (25) (3.4)	<0.01
+ poly(I:C)	55	0.012 ± 0.002 (18) (0.008)	0.015 ± 0.002 (76) (0.013)	3.3 ± 1.9 (6) (3.3)	<0.01
$P2X4^{HA}$Y378A	126	0.018 ± 0.001 (12) (0.38)	0.013 ± 0.002 (68) (0.018)	9.8 ± 6.5 (20) (3.0)	<0.01
+ dynasore	100	0.011 ± 0.003 (12) (0.009)	0.012 ± 0.001 (62) (0.01)	4.9 ± 0.8 (20) (3.5)	<0.01
+ SB203580	115	0.007 ± 0.002 (9) (0.006)	0.010 ± 0.002 (53) (0.013)	3.4 ± 0.5 (38) (3.0)	<0.01
+ apyrase[b]	70	0.002 ± 0.001 (9) (0.002)	0.022 ± 0.003 (63) (0.02)	3.6 ± 0.8 (28) (3.6)	<0.01
$P2X4^{HA}$ in HEK293 cells	181	0.007 ± 0.002 (7) (0.01)	0.018 ± 0.005 (10) (0.022)	9.59 ± 1.4 (83) (1.8)	<0.01
Studies with $P2X2^{FLAG}$ in microglia					
$P2X2^{FLAG}$[c]	225	0.003 ± 0.001 (12) (0.004)	0.009 ± 0.001 (48) (0.013)	2.80 ± 0.39 (40) (4.1)	<0.01
+ LPS[b] + $P2X2^{FLAG}$	65	0.007 ± 0.001 (11) (0.008)	0.007 ± 0.002 (37)) (0.007)	2.40 ± 0.41 (52) (2.4)	<0.01

[a] Paired t tests between linear mobile D and linear lowly mobile D receptors for each experiment are shown.
[b] LPS, fibronectin, and apyrase treatment did not change the diffusion coefficient for any of the trajectory types ($p > 0.05$ relative to control with unpaired Student's t tests). However, LPS and fibronectin reduced the proportion of linear mobile $P2X4^{HA}$ receptors relative to $P2X4^{HA}$ under control settings in microglia (Fig. 8). Note that the units of D for the linear slowly mobile pool are scaled by 10^{-4} as described in the column title.
[c] $P2X2^{FLAG}$ receptors displayed slower mobility than $P2X4^{HA}$ receptors ($p < 0.01$) under control conditions in microglia.

($n = 52$; Fig. 7*D*; Table 2). Interestingly, although the increase in $P2X4^{HA}$ mobility triggered by ATP returned to base-line levels as the receptors desensitized (Fig. 6*C*), the increase in mobility triggered by ionomycin did not and remained significantly elevated for the duration of the ionomycin application (Fig. 7*D*). We also determined that ionomycin elevated microglial calcium levels to ~0.8 μM (Table 3). Along with the calcium-free and BAPTA experiments, the ionomycin experiments show that elevations in cytosolic calcium are both necessary (Fig. 6) and sufficient (Fig. 7*D*) to increase the mobility of $P2X4^{HA}$ receptors in microglia processes.

We next explored whether ATP-evoked changes in $P2X4^{HA}$ receptor mobility were different in activated microglia, because this represents an alternative state of these cells in disease settings. We used LPS (1 μg/ml) to trigger microglial cell activation (25) and found that the ability of ATP to elevate $P2X4^{HA}$ receptor mobility was completely abolished (Fig. 7*E*).

Altered $P2X4^{HA}$ Receptor Lateral Diffusion in Activated Microglia Due to p38 MAPK—Our finding that the ability of ATP to regulate $P2X4^{HA}$ receptor mobility was abolished in activated microglia prompted us to determine whether basal $P2X4^{HA}$ receptor mobility was regulated. To explore this, we studied $P2X4^{HA}$ receptors in microglia by using TLR4 receptor ligands to trigger microglial activation (Fig. 8*A*) (25). We used fibronectin (10 μg/ml) as this is an endogenous mediator of microglial activation *in vivo* and LPS (1 μg/ml) because this is a well established experimental tool (55).

We found several interesting effects of microglial activation on basal $P2X4^{HA}$ mobility. First, both LPS and fibronectin reduced the number of slowly mobile $P2X4^{HA}$ receptors from ~30 to ~5% as revealed by analysis of the cumulative frequency plots of D (*open arrow* in Fig. 8, *B, D,* and *E*; Table 1; $n = 141$ and 61, respectively). Note Fig. 8*E* shows a scatter plot of all the data points for each experiment as well as a convenient summary in the form of a *bar graph* as means ± S.E. Second, neither LPS nor fibronectin changed D for mobile $P2X4^{HA}$ receptors showing that the effect on the slowly mobile receptors was selective (*closed arrow* in Fig. 8*B*; Table 1). Third, we used minocycline (200 μg/ml; $n = 109$) to inhibit the signaling cascade downstream of TLR4 receptor activation (Fig. 8*A*) and found it reversed the effect of LPS on $P2X4^{HA}$ receptors, but again this did not affect D for the mobile receptors (Fig. 7*C*; Table 1). Fourth, the effect of LPS was reversed by SB203580 (Fig. 8*C*; 10 μM; $n = 109$), a specific inhibitor of p38 MAPK (Fig. 8*A*) that is a known effector of TLR4 activation (56). Fifth, the effect of fibronectin and LPS was mimicked by poly(I:C) (an agonist of TLR3 receptors) that activates p38 MAPK independently of TLR4 receptor activation (Fig. 8, *C* and *D*; $n = 5$; Table 1) (57). Sixth, blocking p38 MAPK increased the numbers of slowly mobile receptors to 42% (Fig. 8, *D* and *E*). Taken together, these data show that the pool of slowly mobile $P2X4^{HA}$ receptors is under the bidirectional control of p38 MAPK in microglia. These findings are important because p38 MAPK is involved in the microglial response during pathology (56).

In light of our findings indicating a role for p38 MAPK in basal mobility of $P2X4^{HA}$ receptors, we next determined whether this kinase was also involved in the elevated mobility triggered by ATP applications (Fig. 6). We found that blocking p38 MAPK with SB203580 did not affect the ability of ATP to elevate $P2X4^{HA}$ receptor mobility (Table 2) indicating that the mechanisms that underlie basal and ATP-evoked changes in lateral diffusion are distinct in their requirement for p38 MAPK.

We performed one additional set of experiments in relation to Fig. 7*E* showing that LPS treatment blocks the ability of ATP to increase $P2X4^{HA}$ mobility and in relation to the finding that LPS changed basal $P2X4^{HA}$ mobility (Fig. 8). We thus determined whether microglia activated by LPS when the p38 MAPK pathway was blocked (with minocycline) would "rescue" the ability of ATP stimulation to increase $P2X4^{HA}$ mobility. We found this was not the case (Fig. 7*F*). This also implies that the acute effect of ATP to increase $P2X4^{HA}$ mobility does not need the p38 MAPK pathway in any measurable manner.

We also evaluated if known P2X4 receptor endocytic mechanisms (18) contributed to basal lateral diffusion. Consistent with FRAP data (Fig. 1), $P2X4^{HA}$ receptor lateral diffusion was

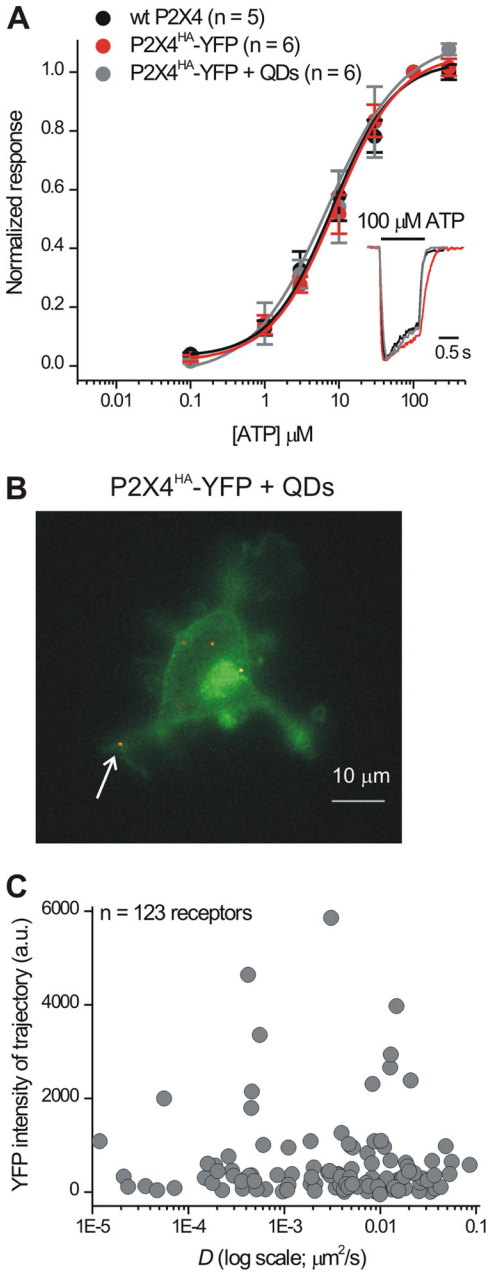

FIGURE 5. **No obvious relationship between diffusion coefficient and YFP intensity over the trajectory area for QD-labeled P2X4^{HA}-YFP receptors.** *A,* normalized concentration-effect curves for ATP at WT P2X4, P2X4^{HA}-YFP, and QD-labeled P2X4^{HA}-YFP receptors in microglia (100 pM QDs were used to ensure that most receptors were bound to QDs; n = 8, 6, and 6). The *inset* shows normalized representative 100 μM ATP-evoked currents from the three concentration-effect curves. *B* shows a maximum projection over time of a microglial cell expressing P2X4^{HA}-YFP receptors and labeled with QDs. The *arrow* points to QD-labeled P2X4^{HA} receptors on processes like the ones that we analyzed in this study. *C, graph* shows the diffusion coefficient D plotted against the YFP intensity measured at the exact same area covered by each QD trajectory (n = 123). No correlation between the two parameters was apparent.

not altered by strategies known to impair P2X4 endocytosis (Y378A mutants and 80 μM dynasore; Table 1).

P2X4^{HA} Receptor Mobility Is Not Regulated by Endogenous ATP in Microglial Cultures—If basal P2X4 receptor mobility is regulated by endogenous ATP release, then we would expect D in the absence of ATP to be lower under conditions that abolish the effects of exogenous ATP (Table 2). We found that D for the corralled linear mobile fraction and for the linear slowly mobile fraction was not lower than control conditions for cells dialyzed with BAPTA or for P2X4^{HA} receptors carrying K67A mutations (Table 4). We next directly explored regulation by endogenous ATP release by measuring basal P2X4^{HA} receptor mobility in cells treated and incubated with extracellular nucleotidase (apyrase at 10 units/ml) (58). Table 4 shows that basal P2X4^{HA} mobility was not affected by apyrase.

We repeated key experiments from the preceding sections with P2X2 receptors to determine whether the responses were P2X4-specific and thus directly explored the possibility that they may represent general effects such as changes in plasma membrane tortuosity. To this end, we used previously characterized P2X2^{FLAG} receptors (Fig. 2*A*) (32). The distinct P2X4^{HA} receptor diffusion coefficients in the plasma membrane of microglia (Fig. 4) were subunit-specific because P2X2^{FLAG} receptors labeled with QDs displayed more slowly mobile receptors (45%) than did P2X4^{HA} receptors (23%) (Table 1). Also, the mobile P2X2^{FLAG} receptors had a lower D at 0.009 ± 0.001 $\mu m^2/s$ (n = 199) in relation to P2X4^{HA} receptors ($p <$ 0.01), and D was not increased or decreased in activated microglia (triggered by LPS; n = 58; Table 1). Moreover, we found that QD-labeled P2X2^{FLAG} receptors did not show any ATP-dependent increase in mobility when expressed in microglia (Table 2), even though the ATP-evoked currents (−22 ± 2 pA/pF) and the accompanying cytosolic calcium elevations at ~3 μM (n = 8; Table 3) were larger as a result of P2X2 receptor activation than as a result of P2X4 receptor activation.

DISCUSSION

The main findings of this study are as follows: (i) P2X4 receptors display distinct types of lateral mobility in microglia; (ii) their mobility increases in a use- and calcium-dependent manner in resting microglia, and (iii) their basal lateral mobility is under the control of p38 MAPK and significantly increased via this pathway in activated microglia. These data show that P2X4 receptors sample more of the microglial plasma membrane when activated by ATP and during the active state that is associated with CNS disorders.

Taken together with previous work (25, 59), our findings show that three trafficking mechanisms regulate P2X4 receptors in microglia. These are the well established mechanisms of dynamin-dependent endocytosis (17, 19, 21, 22), recently reported lysosomal secretion (20, 25, 59), and regulation of lateral mobility dynamics as reported here. Of these, lateral mobility operates on a time scale of seconds that is relevant to P2X4 receptor responses that occur in <1 s and desensitize over ~30 s. Endocytosis occurs over ~21 min (17), and significant lysosomal secretion-mediated up-regulation requires up to 1 h (25).

On the Amplitude of ATP-evoked Currents—Expression of P2X4^{HA} receptors increased ATP-evoked inward currents in resting microglial cells to ~9 pA/pF, *i.e.* to a value ~30-fold higher than the ATP-gated inward currents (~0.3 pA/pF) carried by native P2X4 channels in resting microglia, and similar in magnitude to the ATP-evoked currents of ~5–9 pA/pF carried by native P2X4 channels in LPS-activated microglia (this study and Ref. 25). As reported previously, this increase in native

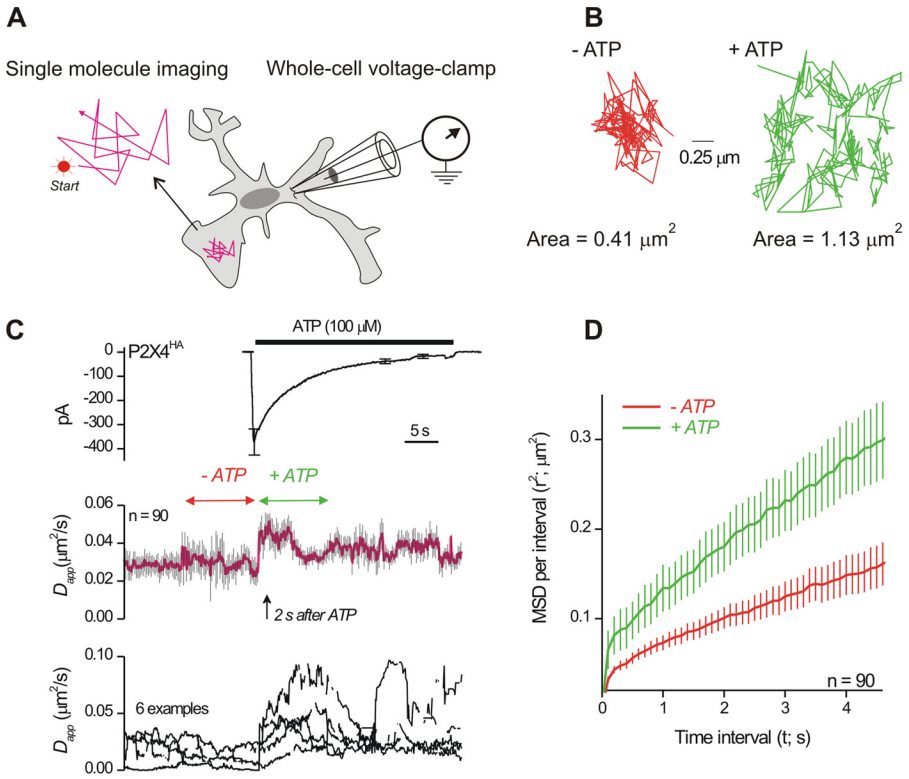

FIGURE 6. **Patch clamp recordings and single-molecule imaging of P2X4^{HA} receptor mobility during ATP applications.** *A,* schematic illustrates the experimental procedure. Microglia expressing P2X4^{HA} receptors were labeled with QDs as described in the text and imaged over time with epifluorescence optics. In most cases, patch clamp electrophysiology was used at the same time to measure transmembrane currents before, during, and after ATP applications. We only imaged QD-labeled P2X4^{HA} receptors on processes because the entire process could be imaged in the same Z-axis optical plane. *B* shows a representative trajectory before and during applications of 100 μM ATP. *C, upper panel* shows the duration of ATP applications as indicated by the *solid bar* and the resulting ATP-evoked inward current in microglia (at −60 mV). The *blue trace* is an average of 15 cells, and the *black lines* represent S.E. The *middle graph* shows a plot of P2X4^{HA} D_{app} over time before and during ATP applications. There was a significant increase in P2X4^{HA} mobility upon ATP applications. We standardized measurements of D_{app} before and during ATP as shown by the *red* and *green arrows* and presented these data in Table 2. The *lower plot* shows six representative examples to provide a feel for the raw data. *D,* MSD plot for the experiments shown in *C* for 30-s periods before and during ATP.

P2X4-mediated currents following LPS treatment reflects increased plasma membrane insertion and retention from a predominant lysosomal pool of P2X4 in resting cells (25). However, it is notable that the maximal ATP-evoked current remains at ~10 pA/pF in cells that are both transfected to express P2X4^{HA} receptors and activated with LPS (Table 1). One might expect that the total current in these latter cells would be at least ~14 pA/pF reflecting the current carried by P2X4^{HA} receptors plus the current carried by the up-regulated native P2X4 receptors. Moreover, if the trafficking of P2X4^{HA} receptors was proportionately up-regulated 30-fold (similar to native P2X4 channels) in resting *versus* LPS-activated cells, one might expect a much greater total current approaching ~300 pA/pF in cells that are both transfected and LPS-stimulated. This was clearly not observed in our experiments, raising several interesting possibilities. The first is that the trafficking and turnover of P2X4^{HA} receptors in microglia differs from that of native P2X4 channels in ways that we do not yet understand or can reliably measure, *i.e.* additional mechanisms remain to be discovered. The second is that the total trafficking/turnover of P2X4 receptors (HA-tagged and native) may be limited by other important factors such as adapters, chaperones, and plasma membrane "binding partners" that are intrinsic to C8-B4 microglial cells. In future studies, it will be important to explore this by examining in detail the transit of tagged and native P2X4 receptors through the microglial cell secretory pathway and also by examining the full repertoire of P2X4 receptor-interacting proteins within microglia.

FRAP and Single-molecule Imaging of P2X4 Receptor Dynamics—We started our evaluations of mobility by using FRAP. However, we found that FRAP was limited in its ability to provide meaningful data because it was dominated by an immobile fraction that was not due to receptor turnover and most likely reflects an intracellular pool. This is consistent with past work demonstrating that P2X4 receptors display substantial intracellular expression, including in vesicles and other organelles (17, 20, 25, 60). Thus, our data show that substantial plasma membrane removal and insertion does not occur over a time course of ~30–60 s (17). Also, the diffraction limit means FRAP is limited by poor *z* axis resolution and thus cannot monitor plasma membrane receptors independently of those within the cell (26, 61), further supporting our data indicating that the FRAP immobile fraction represents stable intracellular fluorescence. In relation to these considerations, cell surface P2X1-GFP receptor turnover was recently studied by FRAP in HEK-293 cells (44). This is likely because these receptors display very fast and extensive turnover (62, 63) that is not shared with P2X4 receptors, which undergo slower molecularly defined clathrin-mediated endocytosis (17, 19, 21, 22).

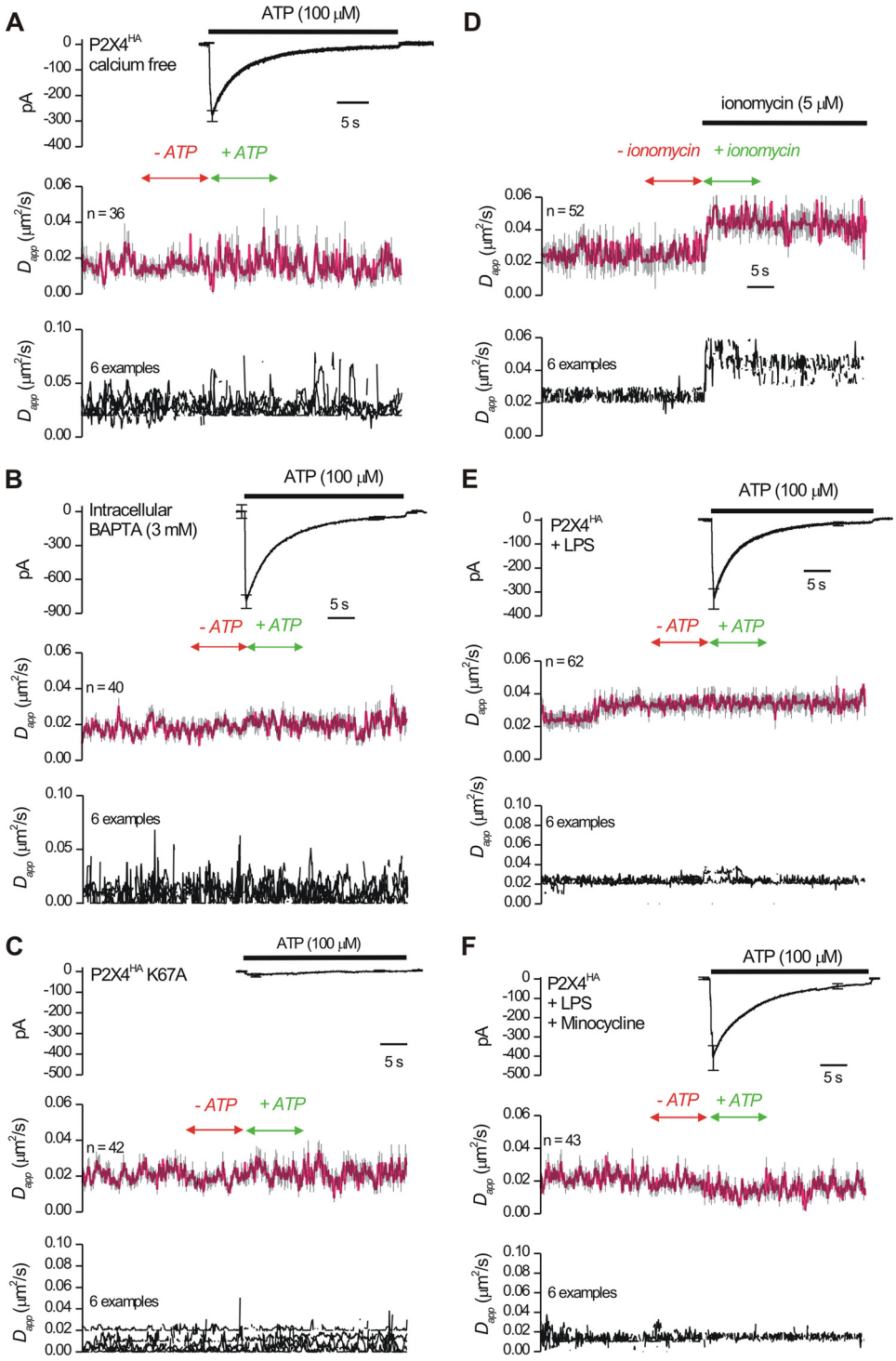

FIGURE 7. **ATP-evoked increases in P2X4^{HA} receptor mobility are triggered by global elevations in intracellular calcium and abolished in activated microglia.** *A,* as in Fig. 6*C* but for cells bathed in calcium-free extracellular buffers. *B,* as in *A* but for cells dialyzed with 3 mM BAPTA via the patch-pipette. Average data are presented in Table 2. *C* shows data such as those shown in Fig. 6 but for cells expressing P2X4^{HA} receptors carrying K67A mutations that impair ATP binding to P2X4 receptors. *D* shows the effect of ionomycin applications. In this case, patch clamp was not performed, but ionomycin was applied at the same time and duration as that for ATP applications (*e.g.* Fig. 6). We started these experiments by determining conditions where ionomycin elevated microglial calcium to levels comparable with those triggered by ATP activation of P2X4^{HA} (0.8 μM; Table 1), which involved increasing the calcium concentration in the extracellular buffer to 8 mM. In a separate series of experiments, we also found that a high extracellular concentration of calcium had no effect on the basal mobility of P2X4^{HA} receptors (0.02 ± 0.001 $\mu m^2/s$ *versus* 0.021 $\mu m^2/s$; Table 1). *E,* ability of ATP to elevate P2X4^{HA} receptor mobility was completely absent in activated microglia whether the p38 MAPK pathway was blocked (*F*) or not (*E*). All the average data are presented in Table 2.

To measure P2X4 receptor lateral mobility directly, we engineered P2X4 receptors to carry epitope tags in the extracellular loop in a region that is surface-exposed (Gln-78) (32–34). This site could be labeled with QDs without altering receptor function or the mobile fraction in FRAP experiments. FRAP-based estimates of diffusion coefficients (47) suggest a value in the

TABLE 2
ATP regulation of P2X4^{HA} receptor mobility

	I_{ATP} (−pA/pF)	Capacitance (pF)	No. of cells	No. of QDs	−ATP D_{app} ($\mu m^2/s$) means ± S.E.	+ATP D_{app} ($\mu m^2/s$) means ± S.E.	p^a
P2X4^{HA} in resting microglia							
Control	9 ± 1	46 ± 2	15	90	0.020 ± 0.002	0.036 ± 0.004	<0.01
Ca^{2+}-free buffer	7 ± 1	48 ± 4	6	36	0.021 ± 0.003	0.019 ± 0.003	0.657
Intracellular BAPTA	23 ± 7	36 ± 7	8	40	0.014 ± 0.003	0.018 ± 0.003	0.411
P2X4^{HA}K67A	0	37 ± 6	5	42	0.007 ± 0.002	0.012 ± 0.003	0.137
Ionomycin	−	−	7	52	0.021 ± 0.003	0.045 ± 0.005	<0.01
Intracellular SB203580	13 ± 3	35 ± 4	8	59	0.014 ± 0.004	0.031 ± 0.002	<0.01
P2X4^{HA} in activated microglia							
+ LPS	10 ± 2	42 ± 2	10	62	0.023 ± 0.003	0.028 ± 0.006	0.397
Studies with P2X2^{FLAG}							
P2X2^{FLAG}	22 ± 2	50 ± 5	5	30	0.01 ± 0.002	0.01 ± 0.001	0.985

[a] *p* values are shown for the paired *t* tests between −ATP and +ATP conditions for measurements of apparent diffusion coefficient (D_{app}) for the experiments indicated (see under "Single Particle Tracking and Data Analysis" and "Results"). I_{ATP} and capacitance were not measured for the ionomycin experiments, which were not performed under voltage clamp (indicated in the table as −).

TABLE 3
Peak change in intracellular calcium levels of microglia under different conditions used in this study

ATP or ionomycin were applied for 30 s at the indicated concentrations, and the peak change in calcium levels occurred within ~10 s.

	Peak $[Ca^{2+}]_i$	*n*
	nM	
100 μM ATP P2X4^{HA}	940 ± 50	9
100 μM ATP P2X4^{HA} Ca^{2+} free	15 ± 90	9
100 μM ATP P2X4^{HA} + LPS	740 ± 50	8
5 μM ionomycin P2X4^{HA}	839 ± 50	8
100 μM ATP P2X2^{FLAG}	3350 ± 55	8

range of 0.01–0.03 $\mu m^2/s$ that is in accord with the value we measured directly with single-molecule imaging at 0.023 $\mu m^2/s$ (Table 1), indicating that QDs do not overtly affect the mobility of receptors (32).

ATP Regulation of Cell Surface P2X4 Receptor Mobility—We capitalized on our past experiences with resting and activated C8-B4 microglia, which represent an *in vitro* system, to explore properties and mechanisms of P2X4 receptors within a native environment (25). Also, it is important to note that lateral mobility can only be adequately studied with single-molecule imaging that can only be performed within optically amenable systems. For practical purposes, this means cell culture (26, 30). With specific relevance to this study, protocols to alter the state of microglia from resting to active have recently been established and extensively tested (25), permitting their use to explore P2X4 receptor mechanisms in distinct microglial states.

We found that receptor lateral mobility increased when the channels were opened and that this required calcium flux and could be mimicked by elevating calcium generally within the cytosol. Importantly, this use- and calcium-dependent increase in mobility did not need p38 MAPK, but it was abolished in activated microglia. The ATP-evoked change in mobility was specific to P2X4 receptors as similar observations were not made with P2X2^{FLAG} receptors in microglia.

Taken together, our data imply that P2X4 receptors sample more of the plasma membrane when the intracellular concentration of calcium is elevated above ~0.4 μM and that this is abolished in disease settings that trigger microglia activation. This response would be of importance in resting microglia that normally express a few cell surface P2X4 receptors by allowing these receptors to sample more of the plasma membrane when activated by ATP. The general nature of P2X4 regulation by calcium also implies that lateral mobility of this receptor may be regulated by other signaling cascades (*e.g.* GPCR pathways) that are involved in the microglial response (64). Also, high concentrations of ATP are released from injured cells (65), and this ATP should be accessible to microglia. From this perspective, studying P2X4 receptor lateral diffusion during *in vitro* injury models to microglial processes would be of interest.

Basal P2X4 Receptor Mobility, Regulation via p38 MAPK—Using single-molecule imaging and tracking, our data provide the first direct measurement of P2X receptor diffusion in the plasma membrane and the first direct proof for the existence of pools of P2X4 receptors with distinct types of mobility. Mobile and slowly mobile pools have also been observed for other receptors in the plasma membrane, but the basis for these pools is not fully known (26). In relation to this, our studies show that the pool of slowly mobile P2X4 receptors is under the constitutive control of p38 MAPK and is altered in activated microglia via this pathway. Thus, increasing p38 MAPK activity with TLR4 and TLR3 ligands decreased the slowly mobile pool, whereas decreasing the activity of this pathway with a specific inhibitor (SB203580) increased the slowly mobile pool.

Our demonstration for a role of p38 MAPK in regulating basal P2X4 receptor lateral mobility is important because this kinase is intimately involved in the microglial response to injury and disease (56). Our data thus suggest that P2X4 receptors sample more of the plasma membrane when microglia are in the activated state. Because activated microglia also have greater numbers of P2X4 receptors in the plasma membrane, this implies that the ability of microglia to respond to ATP would be increased both by elevated numbers of receptors and their increased sampling of the microglial surface. We suggest both these P2X4 receptor mechanisms that are associated with the activated state of microglia may contribute to neuropathic pain when elevated P2X4 responses contribute to the development of this disorder (4).

Cell and P2X Receptor Specificity of Lateral Diffusion—We found no evidence for ATP-evoked changes in P2X4^{HA} receptor mobility in neurons (32), which is in contrast to the findings reported herein for P2X4^{HA} receptors expressed within microglia. We interpret this to indicate that P2X4^{HA} mobility and trafficking are best studied in native cell types on a case-by-case basis, because cells of distinct lineage presumably lack the full

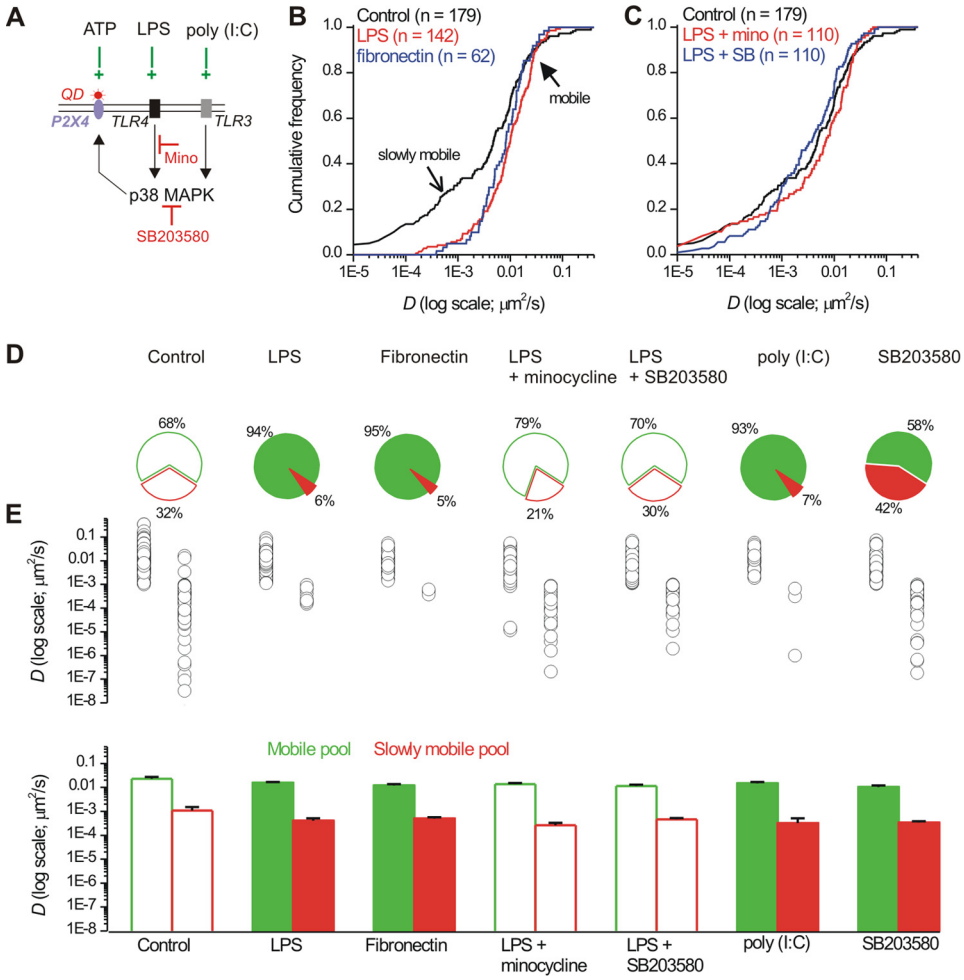

FIGURE 8. **P2X4^{HA} receptor mobility is altered during the activated state of microglia in a p38 MAPK-dependent mechanism.** *A,* schematic illustrates the sites of action of the drugs used in this figure to explore how P2X4^{HA} receptor mobility is altered in activated microglia. ATP (100 μM) activates QD-labeled P2X4^{HA} receptors, and LPS (1 μg/ml) and fibronectin (10 μg/ml) both activate TLR4 receptors, and poly(I:C) (50 μg/ml) activates TLR3 receptors. Activation of TLR4 and TLR3 receptors leads to the activation of a signaling cascade that results in activation of p38 MAPK. This signaling pathway can be blocked by minocycline (200 μg/ml) upstream of p38 MAPK or p38 MAPK can be directly blocked with SB203580 (10 μM). *B, left panel* shows cumulative probability plots of *D* for P2X4^{HA} receptors in resting microglia in relation to measures of *D* for P2X4^{HA} receptors in microglia activated by LPS and fibronectin. Note the distribution shows selective loss of the slowly mobile receptors in activated microglia (*open arrow*), whereas the mobile receptors are the same (*closed arrow*), as revealed by Kolmogorov-Smirnoff analysis. *C,* right-hand cumulative probability plot shows measures for *D* in resting microglia and in cells treated with LPS after blocking TLR4 signaling with minocycline or after blocking p38 MAPK directly with SB203580. In this case, the plots superimpose on that for resting microglia. *D, pie charts* summarize data under the conditions indicated to show the proportion of mobile and slowly mobile receptors. The conditions under which the proportion of mobile to slowly mobile receptors was significantly altered are shown as *filled plots*. *E, scatter plots* and *bar graphs* show the values for *D* in the various conditions shown. Raw data values are shown in Table 1.

TABLE 4

Results for experiments to assess if basal P2X4^{HA} receptor mobility was regulated by endogenous ATP

Apyrase and strategies that abolish the ability of ATP to increase P2X4^{HA} receptor mobility (intracellular BAPTA and K67A mutations) did not decrease *D* for any trajectory type.

	No. of QDs	Corralled *D* (μm^2/s) means ± S.E. (proportion; %)	Linear mobile *D* (μm^2/s) means ± S.E. (proportion; %)	Linear slowly mobile *D* ($\times 10^{-4}$ μm^2/s) means ± S.E. (proportion; %)	p^a
Studies with P2X4^{HA} in microglia					
Control	90	0.005 ± 0.002 (9)	0.024 ± 0.003 (69)	3.2 ± 0.6 (22)	<0.01
Intracellular BAPTA	40	0.0001 ± 0.0003 (13)	0.018 ± 0.003 (62)	3.5 ± 0.7 (25)	<0.01
P2X4^{HA}K67A	42	0.0002 ± 0.0001 (10)	0.014 ± 0.003 (60)	4.0 ± 1.3 (30)	<0.01
+ Apyrase	70	0.002 ± 0.001 (9)	0.022 ± 0.003 (63)	3.6 ± 0.8 (28)	<0.01

[a] In each condition the slowly mobile and mobile fractions were significantly different as expected (see text), and all values for *D* were consistent with experiments reported in Table 1.

repertoire of proteins that normally serve to regulate channel trafficking. We also found strong evidence for receptor specificity; P2X2^{FLAG} receptors did not behave like P2X4^{HA} receptors in microglia (this study), and P2X4^{HA} receptors did not behave like P2X2^{FLAG} receptors in hippocampal neurons (32).

We did not examine P2X4^{HA} receptor mobility in HEK-293 cells for two reasons. First, P2X2 receptors expressed in HEK-293 cells do not display similar lateral mobility compared with when they are expressed in neurons (32). Second, we found that the mobility of P2X4^{HA} receptors in HEK-293 cells was signif-

icantly slower than in microglia (Table 1). Thus, significant differences in lateral mobility between studies in HEK-293 cells and more native cell types for both P2X2 and P2X4 receptors (32) call into question the value of studying P2X receptor trafficking and mobility in HEK-293 cells. We believe this is an important general result from our work on P2X2 and P2X4 receptors that in many ways is obvious with hindsight because it is unlikely that HEK-293 cells contain all the proteins that normally regulate P2X receptors when they are natively expressed.

Important Areas for Future Investigation—In this study, we have assumed that the data collected in cell culture are related to biochemical processes in native microglia. This assumption is based on past work with model cell culture systems and their use in single-molecule work (26) and specifically on work with microglial cultures showing that P2X4 receptors behave in a manner recalling past studies *in vivo* (25, 59). However, the link between the data presented in this study and what occurs in activated microglia *in vivo* merits further detailed work. In future studies, it will be interesting to determine how P2X4 receptor mobility is altered in microglia harvested from mice with neuropathic pain. Such a study will have to await one or more of several advances before it can commence. First, one needs to develop methods to isolate, culture, and transfect microglia from control and neuropathic mice without significantly changing microglial physiology or the function/regulation of P2X4 receptors. As far as we know, no such method yet exists. Second, one would need to develop P2X4 subunit-specific antibodies that target the extracellular domain and develop optical approaches to perform QD-based single-molecule imaging in cell culture or in slices of brain. Third, in what is perhaps the most promising approach, knock-in mice expressing $P2X4^{HA}$ receptors *in vivo* would need to be generated so that the approaches described in this study could be extended to neuropathic pain models. Any one of these advances could permit experiments that may reveal precisely how P2X4 receptor mobility regulation is related to the onset, magnitude, and developmental time course of neuropathic pain.

Our findings with a model cell culture system under known experimental settings reveal two levels of P2X4 receptor mobility regulation. The first is a bidirectional p38 MAPK-dependent mechanism that regulates basal mobile and slowly mobile pools. The second is a calcium-dependent mechanism that regulates receptor diffusion coefficients on a time scale of seconds. In future work, it will be interesting to determine the molecular basis of these signals and tease them apart by evaluating mutant P2X4 receptors. Once distinct mutant receptors lacking either of these two forms of regulation are known, it should then be possible to express them *in vivo*. The study of receptor lateral diffusion is a nascent field, and important roles for receptor lateral diffusion for *in vivo* signaling are expected based on work *in vitro* (26). However, in no case has this possibility been fully evaluated. From this perspective, microglial P2X4 receptor roles in neuropathic pain along with our demonstration of two forms of regulated lateral diffusion offer unique opportunities to experimentally explore how lateral mobility is utilized to tune receptor signaling *in vivo* with direct relevance to disease.

Acknowledgments—We thank all members of the Khakh laboratory for discussions, especially Dr. Esther Richler for detailed comments. We thank Drs. X. Michalet and S. Weiss for useful discussions. We also thank Dr. D. Papazian for comments on an earlier version of this manuscript.

REFERENCES

1. Nakajima, K., and Kohsaka, S. (2005) in *Neuroglia* (Kettenmann, H., and Ransom, B. R., eds) 2nd Ed., pp. 443–453, Oxford University Press, Oxford, UK
2. Graeber, M. B. (2010) Changing face of microglia. *Science* **330,** 783–788
3. Milligan, E. D., and Watkins, L. R. (2009) Pathological and protective roles of glia in chronic pain. *Nat. Rev. Neurosci.* **10,** 23–36
4. Jarvis, M. F. (2010) The neural-glial purinergic receptor ensemble in chronic pain states. *Trends Neurosci.* **33,** 48–57
5. Fields, R. D., and Burnstock, G. (2006) Purinergic signalling in neuron-glia interactions. *Nat. Rev. Neurosci.* **7,** 423–436
6. Khakh, B. S., and North, R. A. (2006) P2X receptors as cell-surface ATP sensors in health and disease. *Nature* **442,** 527–532
7. Egan, T. M., Samways, D. S., and Li, Z. (2006) Biophysics of P2X receptors. *Pflugers Arch.* **452,** 501–512
8. Murrell-Lagnado, R. (2009) More cross-talk between purinergic receptors. *J. Physiol.* **587,** 2713–2714
9. Surprenant, A., and North, R. A. (2009) Signaling at purinergic P2X receptors. *Annu. Rev. Physiol.* **71,** 333–359
10. Tsuda, M., Shigemoto-Mogami, Y., Koizumi, S., Mizokoshi, A., Kohsaka, S., Salter, M. W., and Inoue, K. (2003) P2X4 receptors induced in spinal microglia gate tactile allodynia after nerve injury. *Nature* **424,** 778–783
11. Coull, J. A., Beggs, S., Boudreau, D., Boivin, D., Tsuda, M., Inoue, K., Gravel, C., Salter, M. W., and De Koninck, Y. (2005) BDNF from microglia causes the shift in neuronal anion gradient underlying neuropathic pain. *Nature* **438,** 1017–1021
12. Inoue, K. (2008) Purinergic systems in microglia. *Cell. Mol. Life Sci.* **65,** 3074–3080
13. Ulmann, L., Hatcher, J. P., Hughes, J. P., Chaumont, S., Green, P. J., Conquet, F., Buell, G. N., Reeve, A. J., Chessell, I. P., and Rassendren, F. (2008) Up-regulation of P2X4 receptors in spinal microglia after peripheral nerve injury mediates BDNF release and neuropathic pain. *J. Neurosci.* **28,** 11263–11268
14. Ulmann, L., Hirbec, H., and Rassendren, F. (2010) P2X4 receptors mediate PGE2 release by tissue-resident macrophages and initiate inflammatory pain. *EMBO J.* **29,** 2290–2300
15. Egan, T. M., and Khakh, B. S. (2004) Contribution of calcium ions to P2X channel responses. *J. Neurosci.* **24,** 3413–3420
16. Samways, D. S., and Egan, T. M. (2007) Acidic amino acids impart enhanced Ca^{2+} permeability and flux in two members of the ATP-gated P2X receptor family. *J. Gen. Physiol.* **129,** 245–256
17. Bobanovic, L. K., Royle, S. J., and Murrell-Lagnado, R. D. (2002) P2X receptor trafficking in neurons is subunit-specific. *J. Neurosci.* **22,** 4814–4824
18. Murrell-Lagnado, R. D., and Qureshi, O. S. (2008) Assembly and trafficking of P2X purinergic receptors (Review). *Mol. Membr. Biol.* **25,** 321–331
19. Royle, S. J., and Murrell-Lagnado, R. D. (2003) Constitutive cycling. A general mechanism to regulate cell surface proteins. *BioEssays* **25,** 39–46
20. Qureshi, O. S., Paramasivam, A., Yu, J. C., and Murrell-Lagnado, R. (2007) Regulation of P2X4 receptors by lysosomal targeting, glycan protection, and exocytosis. *J. Cell Sci.* **120,** 3838–3849
21. Royle, S. J., Bobanović, L. K., and Murrell-Lagnado, R. D. (2002) Identification of a noncanonical tyrosine-based endocytic motif in an ionotropic receptor. *J. Biol. Chem.* **277,** 35378–35385
22. Royle, S. J., Qureshi, O. S., Bobanović, L. K., Evans, P. R., Owen, D. J., and Murrell-Lagnado, R. D. (2005) Noncanonical $Y\!XX\!G\Phi$ endocytic motifs. Recognition by AP2 and preferential utilization in P2X4 receptors. *J. Cell*

Sci. **118,** 3073–3080
23. Bowler, J. W., Bailey, R. J., North, R. A., and Surprenant, A. (2003) P2X4, P2Y1, and P2Y2 receptors on rat alveolar macrophages. *Br. J. Pharmacol.* **140,** 567–575
24. Stokes, L., and Surprenant, A. (2009) Dynamic regulation of the P2X4 receptor in alveolar macrophages by phagocytosis and classical activation. *Eur. J. Immunol.* **39,** 986–995
25. Toulme, E., Garcia, A., Samways, D., Egan, T. M., Carson, M. J., and Khakh, B. S. (2010) P2X4 receptors in activated C8-B4 cells of cerebellar microglial origin. *J. Gen. Physiol.* **135,** 333–353
26. Triller, A., and Choquet, D. (2008) New concepts in synaptic biology derived from single-molecule imaging. *Neuron* **59,** 359–374
27. Alcor, D., Gouzer, G., and Triller, A. (2009) Single-particle tracking methods for the study of membrane receptors dynamics. *Eur. J. Neurosci.* **30,** 987–997
28. Gerrow, K., and Triller, A. (2010) Synaptic stability and plasticity in a floating world. *Curr. Opin. Neurobiol.* **20,** 631–639
29. Choquet, D. (2010) Fast AMPAR trafficking for a high frequency synaptic transmission. *Eur. J. Neurosci.* **32,** 250–260
30. Pinaud, F., Clarke, S., Sittner, A., and Dahan, M. (2010) Probing cellular events, one quantum dot at a time. *Nat. Methods* **7,** 275–285
31. Shrivastava, A. N., Triller, A., Sieghart, W., and Sarto-Jackson, I. (2011) Regulation of $GABA_A$ receptor dynamics by interaction with purinergic $P2X_2$ receptors. *J. Biol. Chem.* **286,** 14455–14468
32. Richler, E., Shigetomi, E., and Khakh, B. S. (2011) Neuronal P2X2 receptors are mobile ATP sensors that explore the plasma membrane when activated. *J. Neurosci.* **31,** 16716–16730
33. Stoop, R., Thomas, S., Rassendren, F., Kawashima, E., Buell, G., Surprenant, A., and North, R. (1999) Contribution of individual subunits to the multimeric $P2X_2$ receptor. Estimates based on methanethiosulfonate block at T336C. *Mol. Pharmacol.* **56,** 973–981
34. Chaumont, S., Jiang, L. H., Penna, A., North, R. A., and Rassendren, F. (2004) Identification of a trafficking motif involved in the stabilization and polarization of P2X receptors. *J. Biol. Chem.* **279,** 29628–29638
35. Khakh, B. S., and Egan, T. M. (2005) Contribution of transmembrane regions to ATP-gated P2X2 channel permeability dynamics. *J. Biol. Chem.* **280,** 6118–6129
36. Young, M. T., Fisher, J. A., Fountain, S. J., Ford, R. C., North, R. A., and Khakh, B. S. (2008) Molecular shape, architecture, and size of P2X4 receptors determined using fluorescence resonance energy transfer and electron microscopy. *J. Biol. Chem.* **283,** 26241–26251
37. Alliot, F., Marty, M. C., Cambier, D., and Pessac, B. (1996) A spontaneously immortalized mouse microglial cell line expressing CD4. *Brain Res. Dev. Brain Res.* **95,** 140–143
38. Samways, D. S., Khakh, B. S., and Egan, T. M. (2012) Allosteric Modulation of Ca^{2+} flux in ligand-gated cation channel (P2X4) by actions on lateral portals. *J. Biol. Chem.* **287,** 7594–7602
39. Michalet, X., Pinaud, F. F., Bentolila, L. A., Tsay, J. M., Doose, S., Li, J. J., Sundaresan, G., Wu, A. M., Gambhir, S. S., and Weiss, S. (2005) Quantum dots for live cells, *in vivo* imaging, and diagnostics. *Science* **307,** 538–544
40. Pinaud, F., Michalet, X., Iyer, G., Margeat, E., Moore, H. P., and Weiss, S. (2009) Dynamic partitioning of a glycosylphosphatidylinositol-anchored protein in glycosphingolipid-rich microdomains imaged by single-quantum dot tracking. *Traffic* **10,** 691–712
41. Michalet, X. (2010) Mean square displacement analysis of single-particle trajectories with localization error. Brownian motion in an isotropic medium. *Physical. Rev.* Oct;82(4 Pt 1):041914
42. Saxton, M. J. (1993) Lateral diffusion in an archipelago. Single-particle diffusion. *Biophys. J.* **64,** 1766–1780
43. Khakh, B. S., Burnstock, G., Kennedy, C., King, B. F., North, R. A., Séguéla, P., Voigt, M., and Humphrey, P. P. (2001) International Union of Pharmacology. XXIV. Current status of the nomenclature and properties of P2X receptors and their subunits. *Pharmacol. Rev.* **53,** 107–118
44. Lalo, U., Allsopp, R. C., Mahaut-Smith, M. P., and Evans, R. J. (2010) P2X1 receptor mobility and trafficking. Regulation by receptor insertion and activation. *J. Neurochem.* **113,** 1177–1187
45. Lalo, U., Roberts, J. A., and Evans, R. J. (2011) Identification of human P2X1 receptor-interacting proteins reveals a role of the cytoskeleton in receptor regulation. *J. Biol. Chem.* **286,** 30591–30599
46. Lippincott-Schwartz, J., Snapp, E., and Kenworthy, A. (2001) Studying protein dynamics in living cells. *Nat. Rev. Mol. Cell Biol.* **2,** 444–456
47. Richler, E., Chaumont, S., Shigetomi, E., Sagasti, A., and Khakh, B. S. (2008) Tracking transmitter-gated P2X cation channel activation *in vitro* and *in vivo*. *Nat. Methods* **5,** 87–93
48. Shigetomi, E., Kracun, S., Sofroniew, M. V., and Khakh, B. S. (2010) A genetically targeted optical sensor to monitor calcium signals in astrocyte processes. *Nat. Neurosci.* **13,** 759–766
49. Kawate, T., Michel, J. C., Birdsong, W. T., and Gouaux, E. (2009) Crystal structure of the ATP-gated $P2X_4$ ion channel in the closed state. *Nature* **460,** 592–598
50. Priel, A., and Silberberg, S. D. (2004) Mechanism of ivermectin facilitation of human P2X4 receptor channels. *J. Gen. Physiol.* **123,** 281–293
51. Saxton, M. J., and Jacobson, K. (1997) Single-particle tracking. Applications to membrane dynamics. *Annu. Rev. Biophys. Biomol. Struct.* **26,** 373–399
52. Jiang, L. H., Rassendren, F., Surprenant, A., and North, R. A. (2000) Identification of amino acid residues contributing to the ATP-binding site of a purinergic P2X receptor. *J. Biol. Chem.* **275,** 34190–34196
53. Jiang, L. H., Kim, M., Spelta, V., Bo, X., Surprenant, A., and North, R. A. (2003) Subunit arrangement in P2X receptors. *J. Neurosci.* **23,** 8903–8910
54. Ennion, S., Hagan, S., and Evans, R. J. (2000) The role of positively charged amino acids in ATP recognition by human $P2X_1$ receptors. *J. Biol. Chem.* **275,** 29361–29367
55. Nasu-Tada, K., Koizumi, S., Tsuda, M., Kunifusa, E., and Inoue, K. (2006) Possible involvement of increase in spinal fibronectin following peripheral nerve injury in up-regulation of microglial P2X4, a key molecule for mechanical allodynia. *Glia* **53,** 769–775
56. Cuadrado, A., and Nebreda, A. R. (2010) Mechanisms and functions of p38 MAPK signaling. *Biochem. J.* **429,** 403–417
57. Town, T., Jeng, D., Alexopoulou, L., Tan, J., and Flavell, R. A. (2006) Microglia recognize double-stranded RNA via TLR3. *J. Immunol.* **176,** 3804–3812
58. Bowser, D. N., and Khakh, B. S. (2007) Vesicular ATP is the predominant cause of intercellular calcium waves in astrocytes. *J. Gen. Physiol.* **129,** 485–491
59. Boumechache, M., Masin, M., Edwardson, J. M., Górecki, D. C., and Murrell-Lagnado, R. (2009) Analysis of assembly and trafficking of native P2X4 and P2X7 receptor complexes in rodent immune cells. *J. Biol. Chem.* **284,** 13446–13454
60. Fountain, S. J., Parkinson, K., Young, M. T., Cao, L., Thompson, C. R., and North, R. A. (2007) An intracellular P2X receptor required for osmoregulation in *Dictyostelium discoideum*. *Nature* **448,** 200–203
61. Jaiswal, J. K., and Simon, S. M. (2007) Imaging single events at the cell membrane. *Nat. Chem. Biol.* **3,** 92–98
62. Ennion, S. J., and Evans, R. J. (2001) Agonist-stimulated internalization of the ligand-gated ion channel $P2X_1$ in rat vas deferens. *FEBS Lett.* **489,** 154–158
63. Dutton, J. L., Poronnik, P., Li, G. H., Holding, C. A., Worthington, R. A., Vandenberg, R. J., Cook, D. I., Barden, J. A., and Bennett, M. R. (2000) $P2X_1$ receptor membrane redistribution and down-regulation visualized by using receptor-coupled green fluorescent protein chimeras. *Neuropharmacology* **39,** 2054–2066
64. Koizumi, S., Shigemoto-Mogami, Y., Nasu-Tada, K., Shinozaki, Y., Ohsawa, K., Tsuda, M., Joshi, B. V., Jacobson, K. A., Kohsaka, S., and Inoue, K. (2007) UDP acting at P2Y6 receptors is a mediator of microglial phagocytosis. *Nature* **446,** 1091–1095
65. Cook, S. P., and McCleskey, E. W. (2002) Cell damage excites nociceptors through release of cytosolic ATP. *Pain* **95,** 41–47